pubs.acs.org/Biomac

Article

Iterative RAFT-Mediated Copolymerization of Styrene and Maleic Anhydride toward Sequence- and Length-Controlled Copolymers and Their Applications for Solubilizing Lipid Membranes

Randy D. Cunningham,[‖] Adrian H. Kopf,[‖] Barend O. W. Elenbaas, Bastiaan B.P. Staal, Rueben Pfukwa, J. Antoinette Killian,* and Bert Klumperman*

Cite This: *Biomacromolecules* 2020, 21, 3287−3300

Read Online

ACCESS | Metrics & More | Article Recommendations | Supporting Information

ABSTRACT: The use of poly(styrene-*co*-maleic acid) (SMA) for the solubilization of lipid membranes and membrane proteins is becoming more widespread, and with this, the need increases to better understand the chemical properties of the copolymer and how these translate into membrane solubilization properties. SMA comes in many different flavors that include the ratio of styrene to maleic acid, comonomer sequence distribution, average chain length, dispersity, and potential chemical modifications. In this work, the synthesis and membrane active properties are described for 2:1 (periodic) SMA copolymers with M_w varying from ∼1.4 to 6 kDa. The copolymers were obtained via an iterative RAFT-mediated radical polymerization. Characterization of these polymers showed that they represent a well-defined series in terms of chain length and overall composition ($F_{MAnh} \sim 0.33$), but that there is heterogeneity in comonomer sequence distribution ($F_{MSS} \sim 0.50$) and some dispersity in chain length ($1.1 < Đ < 1.6$), particularly for the larger copolymers. Investigation of the interaction of these polymers with phosphatidylcholine lipid self-assemblies showed that all copolymers inserted equally effectively into lipid monolayers, independent of the copolymer length. Nonetheless, smaller polymers were more effective at solubilizing lipid bilayers into nanodiscs, possibly because longer polymers are more prone to become intertwined with each other, thereby hampering their solubilization efficiency. Nanodisc sizes were independent of the copolymer length. However, nanodiscs formed with larger copolymers were found to undergo slower lipid exchange, indicating a higher stability. The results highlight the usefulness of having well-defined copolymers for systematic studies.

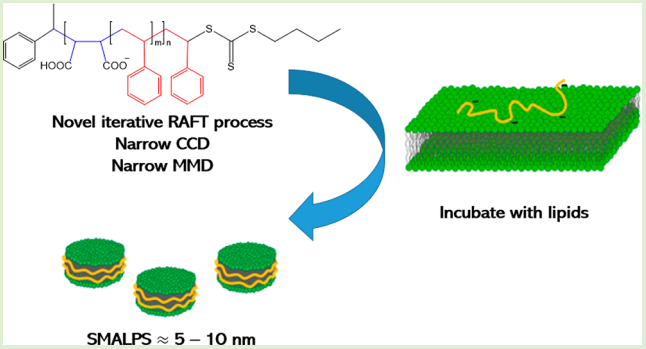

INTRODUCTION

Cells and organelles are surrounded by a semipermeable lipid membrane which is home to a myriad of membrane proteins (MPs) that are responsible for a variety of essential cellular processes.[1] A common first step in studying these MPs consists of their extraction from the native membrane environment by using detergents. However, this extraction method has the disadvantage that the detergents do not accurately mimic the native environment of the MPs.[2] As a result, the MPs to some extent tend to lose their tertiary structure and functionality. In spite of significant developments in design and synthesis of detergents with improved properties,[3] the loss of a native environment remains a weak point of detergent extraction. About a decade ago, a major breakthrough was realized in the isolation of MPs.[4] This breakthrough entails the use of amphiphilic copolymers consisting of styrene and maleic acid units. These copolymers spontaneously insert into membranes and break them up into lipid nanodiscs, stabilized by an annulus of copolymers.[5,6] In this process, MPs are directly transferred to nanodiscs with a diameter in the order of 10 nm, in which the MPs are surrounded by the closely associated lipids that form their native environment.[7−9] As a result, the MPs isolated inside the native nanodiscs are more stable, largely functional and retain their tertiary structure.[10,11]

The commercially available poly(styrene-*co*-maleic acid) (SMA) products have a relatively low molar mass [weight average molecular weight (M_w) ∼10 kDa] and a high dispersity that is characteristic for a polymer synthesized via conventional radical polymerization ($Đ \sim 2$). Unfortunately, this means that commercially available SMA copolymers have a broad molar mass distribution (MMD). This high dispersity is likely to affect the activity of SMA because polymer length has been

Received: May 12, 2020
Revised: July 16, 2020
Published: July 16, 2020

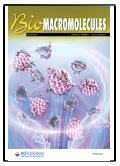

https://dx.doi.org/10.1021/acs.biomac.0c00736
Biomacromolecules 2020, 21, 3287−3300

shown to play a key role in membrane solubilization. Relatively small SMA copolymers with a M_w of ≤10 kDa were found to be more efficient solubilizers than their larger counterparts and the resulting nanodiscs were found to exhibit more dynamic properties.[12−14] In addition to molar mass, the chemical composition is an important parameter for membrane solubilization,[14−17] with several studies showing that a styrene-to-maleic acid ratio of 2:1 is most effective for nanodisc formation.[13,15,16,18] Finally, yet another parameter that may be relevant for membrane solubilization is the chemical composition distribution (CCD) of SMA copolymers. However, not much is known about its role, given that it cannot be controlled in a regular synthesis. For these reasons we thought it of interest to synthesize SMA copolymers with variable molar mass, narrow MMD and narrow CCD and investigate their membrane solubilizing properties.

The synthesis of polymers with a narrow MMD is enabled by a range of techniques that are collectively referred to as reversible deactivation radical polymerization (RDRP). For the synthesis of poly(styrene-*co*-maleic anhydride) (SMAnh), which is the parent copolymer for SMA, two RDRP techniques have successfully been applied. The first one is nitroxide-mediated polymerization[19,20] and the second one is reversible addition−fragmentation chain transfer (RAFT)-mediated polymerization.[21] In nearly all cases that have been reported until now, the focus was either on alternating SMAnh copolymers or on block copolymers with an alternating SMAnh block and a polystyrene block. The only exception that we are aware of is a recent publication in which gradient SMAnh is synthesized with variable steepness of the gradient.[22] These RAFT-made block and gradient copolymers have conveniently low dispersities and furthermore, like the commercially available SMA products, they are capable of inducing formation of nanodiscs in membrane solubilization experiments. However, the RAFT-made copolymers synthesized thus far all have the disadvantage that they are not homogeneous in composition along the backbone.[22−25]

Here we explored a new approach to synthesize non-alternating SMAnh via an iterative RAFT-mediated polymerization reaction. Through this process it is theoretically possible to obtain periodic 2:1 SMAnh copolymers of various average sizes with both narrow MMD and CCD. The polymers were subsequently hydrolyzed to SMA and tested with respect to their efficiency to solubilize model phosphatidylcholine lipid membranes and their influence on the properties of the resulting nanodiscs, often referred to as SMALPs.[26,27] The results highlight the importance of systematic studies on well-defined systems to gain insight into fundamental principles that govern nanodisc formation by SMA copolymers.

MATERIALS AND METHODS

Chemicals and Reagents. Styrene monomer was obtained from Sigma-Aldrich (St. Louis, US) and passed through a basic aluminium oxide (Sigma-Aldrich) column prior to use to remove the inhibitor. Maleic anhydride (Sigma-Aldrich) was recrystallized from toluene and purified by sublimation prior to use. 2,2′-Azobis(2-methylpropionitrile) (AIBN) (Sigma-Aldrich) was recrystallized from ethanol and dried under vacuum at room temperature overnight before use. Triethylamine and 1-bromoethylbenzene were obtained from Sigma-Aldrich and used without any prior purification. All other reagents were used as received. Commercially available SMAnh copolymer, Xiran SZ 30010 [ratio styrene/maleic anhydride (STY/MA) ∼ 2, M_w ∼ 9.1 kDa, number average molecular weight (M_n) ∼ 3.5 kDa, dispersity ($Đ$) ∼ 2.6], was a kind gift from Polyscience (Polyscope, Geleen, NL). SMA2000 (ratio STY/MA ∼ 2, M_w ∼ 7.5 kDa, M_n ∼ 3 kDa, $Đ$ ∼ 2.5) was obtained from TOTAL Cray Valley (Puteaux, FR). Phospholipids (≥99% purity): 1,2-dimyristoyl-*sn*-glycero-3-phosphocholine (di-14:0 PC, DMPC), 1,2-dipalmitoyl-*sn*-glycero-3-phosphocholine (di-16:0 PC, DPPC), 1,2-distearoyl-*sn*-glycero-3-phosphocholine (di-18:0 PC, DSPC), and 1,2-dimyristoyl-*sn*-glycero-3-phosphoethanolamine-*N*-(lissamine rhodamine B sulfonyl) (*N*-rhodamine di-14:0 PE) were purchased from Avanti Polar Lipids (Alabaster, US). For MALDI-ToF-MS measurements, *trans*-2-3-(4-*tert*-butylphenyl)-2-methyl-2-propenylidenemalononitrile (DCTB, Sigma-Aldrich) and 2,5-dihydroxybenzoic acid (DHB, Bruker Daltonics) were used without further purification.

Synthesis of RAFT Agent: Butyl-(1-phenylethyl) Trithiocarbonate.[28] To a 250 mL round-bottom flask containing a Teflon coated stirrer bar were added 1-butanethiol (5.010 g, 56 mmol), carbon disulfide (8.450 g, 111 mmol), and chloroform (40 mL). Triethylamine (11.217 g, 111 mmol) was then added dropwise while stirring, and the reaction was left to react for 5 h at room temperature. 1-Bromoethylbenzene (10.360 g, 56 mmol) was then added dropwise, and the reaction was left to react overnight at ambient conditions. The reaction mixture was then worked up by successively washing with distilled deionized (ddI) H_2O (2 × 50 mL), 2 M H_2SO_4 (2 × 50 mL), ddI H_2O (2 × 50 mL), and saturated brine (2 × 50 mL). This was followed by drying overnight with anhydrous magnesium sulfate and subsequent filtration. The solvent was then removed by rotary evaporator to give a quantitative yield of a viscous yellow/orange oil. The compound was analyzed by ^{1}H NMR (Figure S1) spectroscopy ($CDCl_3$) and was found to be 96% pure.

^{1}H NMR (300 MHz, $CDCl_3$): δ 7.35−7.40 (m, 2H, m-aromatic), 7.30−7.35 (m, 1H, *p*-aromatic), 7.23−7.28 (m, 2H, *o*-aromatic) 5.36 (q, J = 7.1 Hz, 1H, −SC**H**−), 3.35 (t, J = 7.4 Hz, 2H, −SC**H**$_2$−), 1.77 (d, J = 7.1 Hz, 3H, −S−CH−C**H**$_3$), 1.68 (q, J = 7.4 Hz, 2H, −CH$_2$−C**H**$_2$−CH$_2$−), 1.43 (sext, J = 7.3 Hz, 2H, −CH$_2$−C**H**$_2$−CH$_3$), 0.94 (t, J = 7.3 Hz 3H, −CH$_2$−C**H**$_3$)

Iterative RAFT Polymerizations. To a Schlenk flask containing a Teflon coated stirrer bar were added butyl-(1-phenyl ethyl) trithiocarbonate (BPT) (1.0036 g, 3.71 mmol), styrene (0.7800 g, 7.42 mmol), maleic anhydride (0.3638 g, 3.71 mmol), AIBN (0.1204 g, 0.74 mmol), and dimethylformamide (DMF) (2 mL). The contents were degassed by purging with argon for 30 min before being placed in a pre-heated oil bath at 90 °C for 7 h. The reaction was stopped by exposing the contents to air and allowing it to cool to room temperature. To the flask were then added styrene (0.7800 g, 7.42 mmol), maleic anhydride (0.3638 g, 3.71 mmol), AIBN (0.1204 g, 0.74 mmol), and DMF (2 mL). The contents were degassed by purging with argon for 30 min before being placed in a preheated oil bath at 90 °C for 7 h. The reaction was again stopped by exposing the contents to air and allowing it to cool to room temperature. Various molecular weights were targeted by subsequent similar monomer additions. The polymer was precipitated in a large excess of isopropanol, redissolved in dichloromethane, and precipitated again. The yellow powder was then filtered and dried in vacuo at 50 °C overnight.

SMAnh Copolymer Characterization. ^{1}H and ^{13}C NMR spectra were recorded in $CDCl_3$ or acetone-d_6 using a Varian VXR-Unity spectrometer (300, 400 or 600 MHz). ^{13}C DEPT NMR experiments were recorded using 10% w/v solutions (in acetone-d_6) at 37 °C using a 2 s recycle time.[29]

Size exclusion chromatography (SEC) analysis was used to determine the size (M_n and M_w) and the $Đ$ (= M_w/M_n) of the polymers using a Waters instrument equipped with a Waters 2487 dual λ UV detector, a Waters 1515 isocratic high-performance liquid chromatography (HPLC) pump, a Waters 410 differential refractometer (set at a temperature of 30 °C), a Waters 717 plus autosampler, and a waters in-line degasser. The column setup includes a PLgel 5 μm guard column and two PLgel 5 μm mixed-C columns. The column temperature was set at 30 °C. Tetrahydrofuran (HPLC grade, BHT stabilized) was used as the eluent at a flow rate of 1 mL/min at a pressure of 941 psi. The system was calibrated using narrow polystyrene standards with a molecular weight range of 580−

https://dx.doi.org/10.1021/acs.biomac.0c00736
Biomacromolecules 2020, 21, 3287−3300

3,187,000 Da. Sample concentrations were 2 mg/mL, and all data are reported as polystyrene equivalents.

Matrix-assisted laser-desorption ionization time-of-flight mass spectrometry (MALDI-ToF-MS) was carried out with a Bruker Ultraflex Extreme using a smartbeam II laser (1000 Hz) in positive mode and a scan range (m/z) of 20−5000 amu. Samples were prepared by mixing polymer sample with DCTB in a miniature mortar and pestle. The mixture is applied to the target plate with a spatula. Calibration is carried out with 1 μL polyalanine (5 mg/mL in water) and 1 μL DHB [10 mg/mL in MeOH/water, 1/1 (v/v)] as matrix, which were mixed on the target spot and air dried.

Average Chemical Composition Determination. The average copolymer chemical composition was determined via three independent techniques:

^{1}H NMR spectra were integrated, and values were calculated according to eq 1.

$$F_S = \frac{0.2 \times \delta_{5.90-8.00}}{0.5 \times \delta_{0.80-3.71} - 0.1 \times \delta_{5.90-8.00}} \quad (1)$$

where $\delta_{5.90-8.00}$ is the integral of the aromatic STY protons (5) and $\delta_{0.80-3.71}$ is the integral of the total aliphatic protons [MAnh (2) and STY (3)].

^{13}C NMR spectra were recorded with gated decoupling to remove nuclear Overhauser enhancement. Average composition was calculated from the relative areas of the carbonyl signal at ∼172 ppm and the aromatic signal at 127−144 ppm.

CH_2-subspectra of ^{13}C DEPT NMR were integrated as reported in the literature,[29] and values were manipulated according to eq 2.

$$\frac{F_s}{F_M} = 1 + \frac{2A_{SSS} + A_{SSM+MSS}}{2A_{MSM} + A_{SSM+MSS}}; \qquad F_S = \frac{\frac{F_S}{F_M}}{1 + \frac{F_S}{F_M}} \quad (2)$$

Molecular weight via ^{1}H NMR spectroscopy was calculated according to eq 3.

$$M_n(\text{g mol}^{-1}) = \left(\left(\frac{\int \text{phenyl region}}{5}\right) * M_r(\text{STY})\right) + \left(\left(\frac{\int \text{aliph. region} - \text{STY protons}}{2}\right) * M_r(\text{MAnh}) + M_r(\text{BPT})\right) \quad (3)$$

The methyl group of BPT (δ 0.80−0.95) was first integrated and set to a value of 3. The phenyl and aliphatic regions were then integrated relative to this.

Hydrolysis of SMAnh to SMA. Hydrolysis experiments were performed as previously described.[30] Briefly, the SMAnh polymers (0.6 g) were suspended in H_2O to a final concentration of 5% (w/v) containing 1.2 equiv NaOH (relative to maleic anhydride units). The reaction mixture was placed in an autoclave, run for two cycles (each 15 min at 125 °C), and was then left to stir at room temperature for a further 48 h. As the solutions were slightly turbid (particularly for the lower molecular weight polymers), they were washed with Et_2O (3 × 10 mL). SMA copolymers were then precipitated by the addition of 1 M HCl (2.5 mL). Suspensions were centrifuged (12,000g, 10 min, 4 °C) to pellet down the precipitate. The supernatant was decanted off, and the resulting pellets were washed by resuspending in 10 mM HCl (10 mL) and centrifuging (the washing was repeated three times). After the final washing step, the pellets were dried under a stream of nitrogen gas and finally in the vacuum desiccator, which gave the products as yellow solids (yields ∼85%). To dissolve the hydrolyzed products, they were initially suspended in H_2O at a concentration of 10% (w/v), containing 0.6 equiv NaOH to COOH units. After mixing thoroughly, the cleared solution was determined to have a pH of ∼9. The mixtures were then diluted to a final concentration of 5% (w/w). Finally, the solutions were filtered through a 0.2 μm cellulose acetate membrane (VWR), to give the SMA stocks as transparent yellow solutions.

Monolayer experiments. Surface pressure isotherms versus time were recorded for lipid monolayers formed of either DMPC or DSPC upon addition of 20 μL SMA 5% (w/w), yielding a final concentration of ∼0.005% (w/v). Phospholipid monolayers were assembled on an aqueous subphase in a 6 × 5.5 cm compartment of a homemade Teflon trough filled with 19 mL buffer (50 mM Tris−HCl, 150 mM NaCl, pH 8). Aliquots from 0.5 mM phospholipid stock solutions in chloroform were carefully added dropwise to the surface of the buffer solution until an initial surface pressure of 25 mN/m was reached. SMA was injected into the aqueous subphase after at least 2 min of stabilization, and the resulting increase in surface pressure was recorded for at least 30 min using a MicroTrough XS monolayer system (Kibron, Helsinki, Finland). Surface pressure isotherms presented in this study are a result of the average of two independent experiments. All experiments were conducted at ambient temperature in a climate-controlled room (∼21 °C).

Preparation of Multilamellar Vesicles. Phospholipid stock solutions were prepared in chloroform at concentrations of 20 mM. The solvent was removed under a stream N_2 with mild heating (35−40 °C). The resulting lipid film was dried further in a desiccator under vacuum for at least 1 h. Next, the lipid films were hydrated with buffer (50 mM Tris−HCl, pH 8, 150 mM NaCl) to the desired final concentration and equilibrated for at least 30 min at 30 °C for DMPC or 45 °C for DPPC, which for both is at $T > T_m$.[31] Finally, the samples were subjected to 10 freeze−thaw cycles, each consisting of 3 min freezing in a bath of solid CO_2/EtOH and 5 min thawing in a warm water bath at $T > T_m$.

Preparation of Nanodiscs. Dispersions of multilamellar vesicles (MLVs) in solubilization buffer (50 mM Tris−HCl, pH 8, 150 mM NaCl) were mixed with SMA 5% (w/w) (final SMA-to-lipid mass ratio of ∼3) overnight at $T > T_m$, with constant agitation using an Eppendorf shaker (600 rpm). The nonsolubilized material was pelleted down by spinning at 21,000g for 1 h at 4 °C and the supernatant, containing the solubilized lipid material, was collected. Samples that were not analyzed immediately were stored in the fridge (4 °C).

Dynamic Light Scattering. The size of the nanoparticles was determined by dynamic light scattering (DLS) using a Zetasizer nano ZS (Malvern instruments, Worcestershire, UK). Measurements were performed on nanodisc samples containing either DMPC or DPPC at a lipid concentration of ∼1.5 mM, or on SMA only samples at a polymer concentration of 0.5% (w/v). All samples were dispersed in buffer (50 mM Tris−HCl, pH 8, 150 mM NaCl), and experiments performed at 21 °C, after equilibrating for 240 s. Detection of backscattering was performed at an angle of 173°, and the data were processed using the multiple narrow modes as the analysis model. Data were recorded as the average of six experiments, each consisting of at least 12 subruns of 10 s. The reported hydrodynamic size values are obtained from the number distributions, with the assumption that nanodiscs have a spherical shape.

Transmission Electron Microscopy. The morphology and size of the nanodiscs were further investigated by negative stain transmission electron microscopic (TEM). Aliquots of solutions used for DLS analysis were diluted to a lipid concentration of ∼0.7 mM. Carbon-coated copper grids (200 mesh) were glow discharged for 30 s. Sample (5 μL) was applied to the grid and after 60 s blotted off with (ashless) filter paper and subsequently washed, with H_2O and uranyl acetate (UA, 2% in H_2O), and then finally stained with UA for 60 s before blotting dry. Micrographs were taken on a Tecnai T10 electron microscope using an operating voltage of 100 kV. The average size of the nanodiscs was estimated from at least 30 well-defined individual particles.

Kinetics of Solubilization of Phosphatidylcholine Vesicles. Aliquots (700 μL) of 0.5 mM suspensions of DMPC MLVs in solubilization buffer (50 mM Tris−HCl, pH 8, 150 mM NaCl) were left to equilibrate for at least 1 min at 15 °C ($T < T_m$) or 30 °C ($T > T_m$). The temperature was controlled, and the mixture was

https://dx.doi.org/10.1021/acs.biomac.0c00736
Biomacromolecules 2020, 21, 3287−3300

Table 1. Synthetic Routes and Their Respective Advantages and Drawbacks

STY:MA	Synthetic Route	MMD ($Đ$)	CCD (Sequence)	Example[b]
0:1	Batch / CSTR / RAFT	N/A	N/A	N/A
1:0	Batch / CSTR	×	N/A	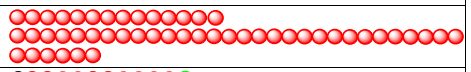
	RAFT	✓	N/A	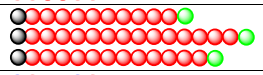
1:1	Batch / CSTR	×	✓	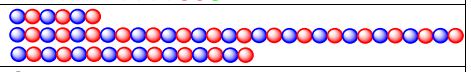
	RAFT	✓	✓	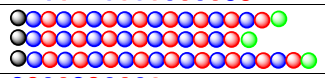
2:1	Batch	×	×	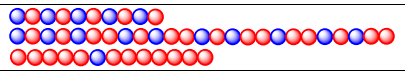
	CSTR	×	✓	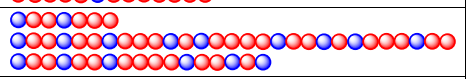
	RAFT	✓	×	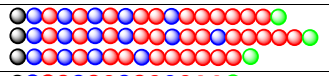
	Iterative RAFT[a]	✓	✓	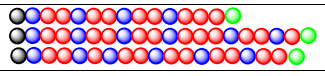

[a]This work. [b]Example of three (co)polymer chains making up a representative batch of polymers for each synthetic strategy shown. Blue dots represent maleic anhydride, red dots represent styrene, and black-green dots represent RAFT agent. The iterative RAFT strategy would combine the advantage of RAFT of having a narrower size distribution and that of CSTR of having a better distributed comonomer sequence.

continuously stirred with a Peltier cuvette holder (Santa Clara, CA, USA). A 15 μL aliquot of SMA 5% (w/w) was added to achieve a final SMA-to-lipid mass ratio of ~3. Solubilization kinetics was followed at a fixed wavelength of 400 nm by monitoring the decrease of the apparent absorbance. The absorbance was measured at a wavelength of 400 nm instead of 350 nm as standard;[5,13] this was done to avoid the interference from the trithiocarbonate RAFT groups that themselves have an absorbance peak at ~315 nm (Figure S2). Absorbance values were recorded every 0.4 s for a total of 15 min using a Lambda 18 spectrophotometer (PerkinElmer, MA, USA).

Rhodamine Fluorescence Dequenching. In 10 mm quartz cuvettes, aliquots of nanodiscs with a total of 2 mM of DMPC/*N*-rhodamine PE (4:1 mol/mol) nanodiscs were diluted to a final volume of 1 mL, yielding a final *N*-rhodamine concentration of 2.5 μM. The solutions were stirred and equilibrated for at least 2 min at 30 °C by using a Peltier cuvette holder (Santa Clara, CA, USA). Fluorescent nanodiscs were excited at 560 nm and mixed with aliquots of unlabeled DMPC nanodiscs. Unlabeled nanodiscs were added to a final lipid molar ratio of 1:5 of labeled-to-unlabeled nanodiscs. Rhodamine was excited at 560 nm (λ_{ex} = 560 nm), and fluorescence was monitored at 592 nm (λ_{em} = 592 nm) for 15 min using a Varian Cary Eclipse fluorescence spectrophotometer (Santa Clara, CA, USA). Experiments were performed using a salt concentration of 50 or 150 mM NaCl and repeated for two independent measurements.

RESULTS

Approach To Synthesize SMAnh Copolymers of Well-Defined Chain Length and with Nonalternating Sequence by Iterative RAFT Polymerization. In order to understand the lack of nonalternating SMAnh via RDRP, one should first consider its conventional radical copolymerization. SMAnh has a strong tendency toward alternating insertion of the monomers.[32] This means that a batch copolymerization of a nonequimolar mixture of styrene and maleic anhydride leads to a copolymer with a broad CCD. In order to synthesize SMAnh with a narrow CCD, the process is conducted in a continuous stirred tank reactor (CSTR).[33] There is a continuous feed of monomer, solvent, and initiator into the (ideally mixed) reactor and a simultaneous extraction of the reaction mixture from the reactor. After circa 3 times the mean residence time in the reactor, a steady state is established, in which a certain overall monomer conversion is reached and a certain ratio of the two comonomers in the steady-state residual monomer mixture is obtained. Because of the steady-state character of the process, the narrowest possible CCD is obtained, the width of which is only dictated by the statistical nature of the copolymerization process, without any influence of the composition drift. The MMD of SMAnh made in this process is not influenced by the residence time distribution in the CSTR because the growth time of an individual chain is very short (order of a second) compared to the mean residence time (order of an hour).

It would be possible to use the CSTR process in order to create a RAFT-mediated nonalternating SMAnh with a narrow CCD. However, in the case of any RDRP process, the growth time of an individual chain spans the duration of the polymerization process. In a CSTR process, that duration is dictated by the residence time distribution in the reactor. In other words, there are volume elements that will spend a very short time in the reactor and other volume elements that spend up to 3 or 4 times the mean residence time in the reactor.[34] Because the molar mass in RDRP is directly related to monomer conversion, which in turn is strongly related to the reaction time, it will be obvious that the MMD of an RDRP-made polymer from a CSTR is largely dictated by the residence time distribution. In practice, this means that such an MMD will have a dispersity close to that of conventional radical polymerization ($Đ \sim 2$).

In summary, the dilemma of making nonalternating SMAnh with a narrow CCD and narrow MMD is that it cannot be conducted in a normal batch reaction because of the

https://dx.doi.org/10.1021/acs.biomac.0c00736
Biomacromolecules 2020, 21, 3287−3300

occurrence of the composition drift and also not in a CSTR because of the residence time distribution (see Table 1 for an overview). As a solution to this dilemma, we propose an iterative process in which nonalternating SMAnh is built up in a stepwise series of chain extensions. Briefly, in order to target SMAnh with a 2:1 styrene-to-maleic anhydride ratio, narrow CCD, and narrow MMD, we performed consecutive additions of 2 equiv of styrene and 1 equiv of maleic anhydride per equivalent of the RAFT agent and a supplemental initiator as a radical source. This procedure is similar to what was previously published for acrylate polymerizations by Perrier and co-workers.[35] The number of monomer additions was dictated by the target molar mass of the copolymer. In the ideal scenario, the applied procedure could lead to sequence-controlled copolymers. In order for that to happen, the probability of monomer addition to the growing chains should be sufficiently discriminatory to prevent deviations from the intended monomer sequence. To be more specific, the addition of maleic anhydride should be very fast after each new monomer addition. Then, the first styrene should also be very fast, which is expected in view of the strongly alternating character of SMAnh. The uncertain factor is the addition of the second styrene. In order to obtain sequence control, the addition of the second styrene should be significantly faster than the third and subsequent styrene additions. Harrison, Perrier, and co-workers have previously pointed at the limitations of precision placement of monomers in an RDRP process.[36] We will come back to this later in this contribution.

Polymers of various average molecular weights were synthesized via the iterative process described above, with details as reported in Table 2. Iterative RAFT polymerization allows us to synthesize nonalternating SMAnh by repetitive addition of 1 maleic anhydride and 2 styrene molecules per RAFT moiety and subsequent repeated addition of monomers after the full conversion of the previously added monomers (see Scheme 1). In this work, we selected 1-phenylethyl as the R-group of the RAFT agent to ensure that maleic anhydride is added first with a high rate.[37] The reaction vessel contains equimolar amounts of the RAFT agent and maleic anhydride. Hence, after the insertion of maleic anhydride into the RAFT agent, styrene is allowed to react because of it being the only monomer left in solution. From previous work, we know that the first styrene addition to a MAnh radical is very fast.[38] Furthermore, on the basis of previous kinetic studies of the conventional radical copolymerization of styrene and maleic anhydride, we believe that the second styrene addition is also slightly faster than subsequent styrene additions.[37] This could possibly lead to the preferred formation of an MSS triad in each chain, which is subsequently chain-extended in the iterative process until the desired chain length is obtained.

In this fashion, we avoid the formation of gradient copolymers, as maleic anhydride and styrene comonomers are periodically added to the reaction vessel.

Table 2. Molar Mass and Dispersity of Synthesized Copolymers

sample code	$(MSS)_n$[a]	$M_{n,target}$ (Da)[a]	$M_{n,NMR}$ (Da)	$M_{n,SEC}$ (Da)	$Đ$
MSS2	2	884	1500	1300	1.1
MSS4	4	1496	2200	2000	1.2
MSS6	6	2109	2800	3000	1.3
MSS7	7	2415	3000	3000	1.3
MSS8	8	2722	3100	3800	1.4
MSS16	16	5173	4100	3700	1.6

[a]Targeted number of (MSS triad) sequence repeats and the corresponding theoretical masses.

Characterization of the Chain Length and Dispersity of the Copolymers. SEC results (Figure S3) indicate good control of MMD as evident by low $Đ$ values (see Table 2). However, an increased molecular weight is accompanied by an increased $Đ$, as can be seen in Table 2 and Figure S3. This gradual increase in $Đ$ could be a sign of progressive termination of growing chains and therefore an increasing fraction of dead copolymer chains.

^{1}H NMR spectroscopy confirms the synthesis of SMAnh, as evidenced by the broad aromatic and aliphatic polymer signals that are very characteristic for SMAnh (Figure 1A).[25] Quantification of the RAFT end-groups is hampered by overlapping polymer signals. The terminal methyl protons belonging to the RAFT Z group were used as a reference as they were the only RAFT-associated protons that were resolved from the polymer backbone. The degree of polymerization (DP) and related number-average molar mass (M_n) values were determined by integrating the polymer peaks relative to the RAFT end-group, whereas the average chemical composition was determined from the ratio between aliphatic and aromatic proton signals in the ^{1}H NMR spectrum. The chemical composition determined by ^{1}H NMR (Figure S4A) spectroscopy was in close agreement with the feed composition of 2 STY:1 MAnh (F_s = 0.66). This composition was confirmed by quantitative ^{13}C NMR spectroscopy (Figure 1B) and is reported in Table 3.

Characterization of Sequence Distribution. Further analysis by ^{13}C DEPT NMR (Figure S4B) spectroscopy revealed the sequence distribution along the polymer backbone. Integration of the methylene subspectrum as reported by Barron et al. yields quantitative information pertaining to the styrene-centered triad distribution (Figure 1B).[29] The

Scheme 1. Iterative BPT RAFT-Mediated Copolymerization of Styrene and Maleic Anhydride, Followed by the Hydrolysis to Poly(styrene-*co*-maleic acid)

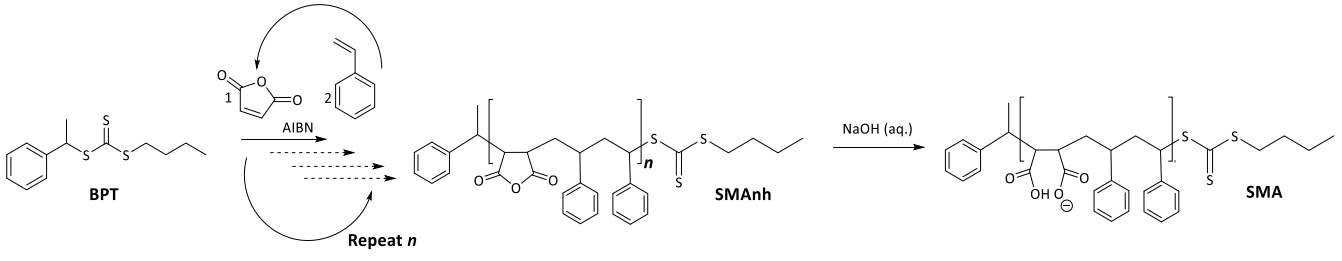

https://dx.doi.org/10.1021/acs.biomac.0c00736
Biomacromolecules 2020, 21, 3287−3300

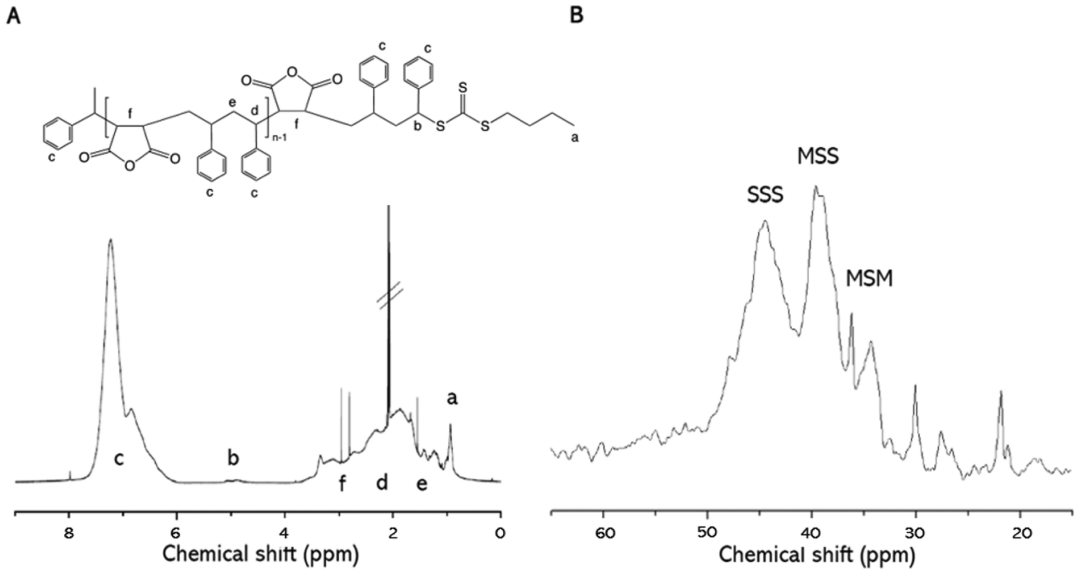

Figure 1. (A) ^{1}H NMR ($CDCl_3$) and (B) ^{13}C DEPT NMR [$(CD_3)_2CO$] (CH_2 subspectrum) spectra of the synthesized copolymer (MSS7).

Table 3. Chemical Composition and Sequence Distribution of Synthesized Copolymers

	F_S			^{13}C DEPT NMR (CH_2 subspectrum)		
sample code	^{1}H NMR	^{13}C NMR	DEPT NMR	F_{MSM}	$F_{MSS/SSM}$	F_{SSS}
MSS2	0.61	0.68	0.68	0.22	0.48	0.29
MSS4	0.60	0.56	0.55	0.28	0.57	0.15
MSS6	0.57	0.62	0.60	0.25	0.50	0.25
MSS7	0.66	0.68	0.69	0.22	0.45	0.33
MSS8	0.52	0.68	0.66	0.27	0.51	0.22
MSS16	0.59	0.70	0.73	0.15	0.42	0.43
SMA2000				0.37	0.50	0.13
Xiran SZ 30010				0.42	0.49	0.09

dominating sequence was found to be the MSS (+SSM) triad. Although there is some scatter in the experimentally determined triad distributions, the fraction of MSS triads is roughly $F_{MSS} \approx 0.50$, whereas those of MSM and SSS are more or less equal at $F_{MSM} \approx F_{SSS} \approx 0.25$ (see Table 3). This holds across all synthesized polymer lengths, suggesting a homogenous CCD. This is, however, far off the targeted MSS as the dominating repeating sequence. The fraction MSS in a conventional SMAnh produced in a CSTR is also around $F_{MSS} \approx 0.50$ (Table 3) and therefore is comparable to the described iterative process.

MALDI-ToF-MS was used to further analyze the SMAnh copolymers. The results of sample MSS2 are shown in Figure 2 as a contour plot, calculated from the MALDI-ToF-MS raw data. The data shown are from the chains that carry the trithiocarbonate chain end. There is a second population of chains that lack the trithiocarbonate end-group, which can either be due to termination events or can be an artifact due to the pulsed laser of the MALDI instrument. Both populations of chains show very comparable composition profiles. As can be seen from the contour plot in Figure 2, there is a distribution in the chain length and chemical composition, although the average is close to the targeted 2:1 STY/MAnh ratio. These results confirm the NMR and SEC results. MALDI-ToF-MS on the longer chains proved to be challenging, which is in line

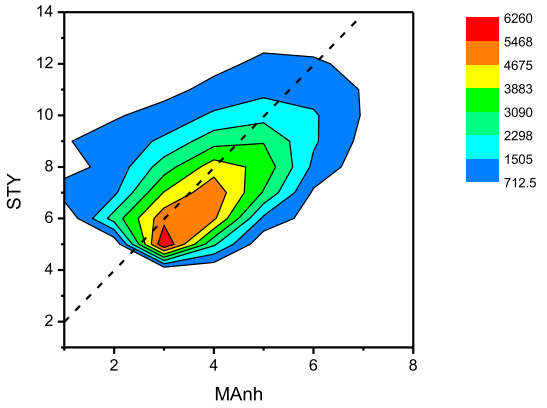

Figure 2. Contour plot based on MALDI-ToF-MS results, showing the number of STY repeat units as a function of the number of MAnh repeat units for sample MSS2. The colors from blue to red denote increasing peak intensities in MALDI-ToF-MS in arbitrary units. The dashed line is the theoretical prediction for a 2:1 STY/MAnh copolymer.

with our earlier experience for SMAnh copolymers. As a consequence, we will not show the MALDI-ToF-MS results for the larger chain lengths.

What Controls the Dispersity and Sequence Distributions of the Copolymers? On the basis of NMR spectroscopy and SEC results, it can be concluded that the copolymers possess a composition close to the targeted $F_{MAnh} = 0.33$ and a molar mass that follows the theoretical predictions. However, the dispersity increases significantly with increasing chain extension steps in the iterative process (see Table 2), and importantly, for all chain lengths, the monomer sequence distribution deviates strongly from the targeted $(MSS)_n$. There are two simultaneous processes that account for the observed behavior.

The first process is the occurrence of irreversible termination of growing chains. Although the alternating copolymerization of STY and MAnh is characterized by high propagation rate coefficients, the homopolymerization of STY has a notoriously low propagation rate constant. After initial optimizations, we decided to work with a relatively high concentration of the

https://dx.doi.org/10.1021/acs.biomac.0c00736
Biomacromolecules 2020, 21, 3287−3300

initiator to arrive at an acceptable polymerization rate in the regime where only STY is left to react. The consequence of the high initiator concentration is that a large and increasing fraction of the copolymer chains are dead. A theoretical assessment of the fraction of dead chains indicates that the fraction could range from 0.32 for the MSS2 sample to 0.79 for the MSS16 sample. These calculations are detailed in the Supporting Information. The gradual increase in dispersity of the samples with increasing chain length is in agreement with the occurrence of irreversible termination.

The second process is the propagation reaction and the degree of control that we can apply to that. As indicated above, the first addition to an electron-rich radical (RAFT agent-derived radical or STY-terminal propagating radical) is by MAnh and is very fast. Similarly, the addition of STY to a MAnh-terminal-propagating radical is also very fast. However, it is what comes next that may lead to deviations from the targeted MSS sequences. The first scenario that can lead to a deviation is the second addition of a MAnh and STY to a chain that has already added monomers in a specific chain extension step. The question at hand is that is it reasonable to expect that all chains adding one MAnh (plus STY) per chain extension step are preferred over some chains adding more than one, whereas others add none? The second scenario is the lack of selectivity for a second STY addition over the addition of the third and more STY units to an individual chain, leaving other chains with no STY to form the desired MSS triad. Detailed kinetic investigations that are beyond the scope of this contribution are currently carried out in our group to elucidate the exact origin of the absence of sequence control in our experiments. For now, we believe that the statistical nature of the copolymerization, where additions are controlled by probabilities, is responsible for the observed monomer sequence distribution. This explanation is in line with the previously mentioned study by Harrison, Perrier, and co-workers.[36]

The copolymers were further analyzed by UV−vis (Figure S2) as well as infrared (IR) (Figure S5) spectroscopy. In both cases, the synthesized SMA copolymers were compared to the commercially available Xiran 30010. All of the copolymers had the characteristic SMA spectrum according to IR[13,39,40] as well as UV in the region 230−280 nm.[24,30,41] The newly synthesized polymers however also had a peak at 315 nm, owing to the RAFT agent on the terminus of the chains. The size of this extra peak relative to the peak at 254 nm (RAFT group vs styrene) also gives an indication that the copolymers increase in the chain length going from MSS2 to MSS16. This is also macroscopically visible when looking at the copolymer solutions (Figure S6), where the smaller copolymers display a more intense yellow color, which is attributed to the higher concentration of the RAFT terminal groups.

Despite the heterogeneity in the monomer sequence and the higher dispersity in the length for the longer copolymers, these SMA copolymers form a very well-defined series in terms of total length and overall composition, suitable for systematic studies. We next investigated their interaction with lipids using several complementary approaches.

Synthesized Copolymers All Have Comparable Insertion into Lipid Monolayers. For the formation of nanodiscs, polymers first need to bind to and insert into the lipid membrane.[5] To investigate the efficiency of this first step in the solubilization process, lipid monolayer experiments were performed. Figure 3A shows that all copolymers insert similarly

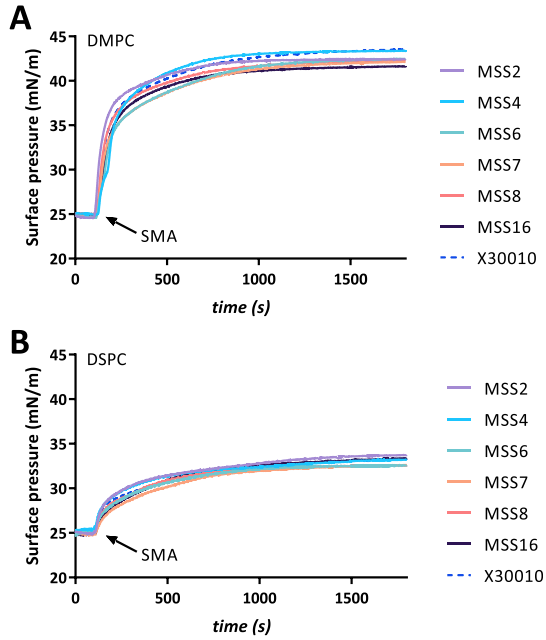

Figure 3. Increase in the surface pressure as caused by the insertion of SMA copolymers in monolayers composed of (A) DMPC and (B) DSPC. The point of SMA addition to the aqueous subphase (50 mM Tris−HCl, 150 mM NaCl, pH 8) is indicated with an arrow. Experiments were conducted at ambient temperature (∼21 °C), with a final SMA concentration of 0.005% (w/v).

well in monolayers of DMPC, which are present in a fluid-like (liquid-expanded) phase.[42,43] The copolymers are highly surface active, increasing the surface pressure to a final pressure of ∼42 mN/m. Experiments on monolayers of DSPC (Figure 3B), which form a gel-like (solid-condensed) phase,[42,43] similarly showed that all copolymers insert equally well, but now only to a final surface pressure of ∼33 mN/m, presumably because of the tighter packing of the lipids. In both cases, the surface activity of the copolymers is comparable to that observed for Xiran 30010. Remarkably, these findings differ from previous results on purified SMA fragments, which showed a larger increase in surface pressure for smaller fragments.[13] Possible reasons for this discrepancy will be discussed later.

Although there is no obvious effect of the polymer length on monolayer insertion, the surface activity of the length fragments in a buffer-only system (Figure S7) showed a very small but systematic trend. Here, smaller copolymers were found to partition more effectively at the water−air interface, thereby disrupting the surface tension slightly more as compared to the longer chain copolymers. Importantly, for all copolymers, a higher final surface pressure was observed in the presence of lipid monolayers as compared to only buffer at the air−water interface, testifying to their strong affinity toward phospholipid molecules (Figure S8). It is also this property that ultimately allows the solubilization and stabilization of MPs.

Faster Solubilization Kinetics Are Observed for SMA Copolymers of Smaller Sizes. The effect of the SMA copolymers on the solubilization process was investigated by turbidimetric analysis using DMPC MLVs. The experiments were performed as described previously.[5] At 30 °C, with the membrane in the fluid (liquid-crystalline) phase, extremely fast solubilization was observed (Figure 4A). All of the copolymers

https://dx.doi.org/10.1021/acs.biomac.0c00736
Biomacromolecules 2020, 21, 3287−3300

induced complete solubilization within 60 s after their addition.

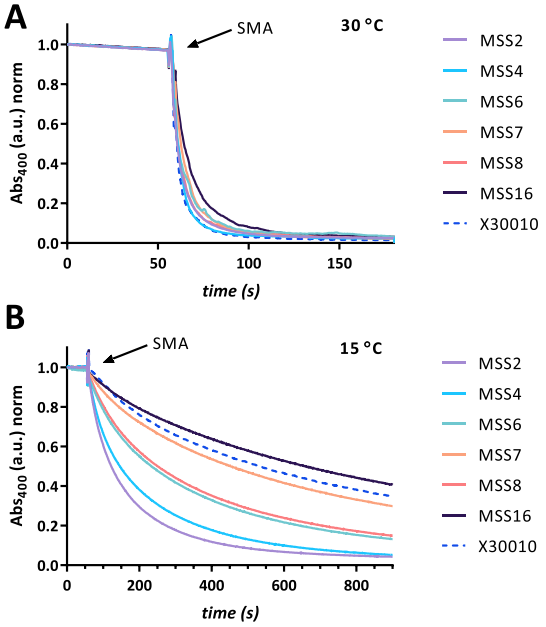

Figure 4. Kinetics of solubilization of DMPC liposomes after the addition of SMA copolymers. Experiments were performed at either (A) 30 °C (n = 1) or (B) 15 °C (n = 5). All measurements were conducted with 0.5 mM lipid and 0.1% (w/v) SMA (final SMA-to-lipid mass ratio of ~3). Data are given as normalized apparent absorbance values at 400 nm, and the curves at 15 °C represent the average value of five independent experiments, with standard deviations (not shown) less than 0.12 a.u. at any time point.

The same experiments were performed at 15 °C, which is below the gel to liquid-crystalline phase transition temperature of these lipids.[31] Figure 4B shows that in this case a general trend does occur, with shorter polymers having faster solubilization kinetics. MSS2 being the smallest polymer had the fastest rate, with complete solubilization at 900 s, whereas the largest polymer, MSS16, was the slowest solubilizer with ~50% solubilization at 900 s. The only deviation from the systematic correlation between solubilization efficiency and size can be seen for MSS7 and MSS8. We do not know the reason for this, but we note that MSS8 is the only copolymer that shows a significant discrepancy for M_n as determined by NMR compared to SEC, while also having a high size dispersity. Xiran 30010 had solubilization kinetics between MSS16 and MSS7, indicating that it follows the same length correlation (Figure S9).

Size of the Formed Nanodiscs Is Independent of the Size of the SMA Copolymer. Next, it was determined whether the length of the copolymers affects the size of the formed nanoparticles. To this end, DMPC MLVs were incubated with the SMA copolymers, and the resulting nanoparticles were characterized by DLS. As can be seen in Figure 5A, there is no correlation between the length of the polymer and the size of the resulting nanodiscs, as all of the discs have a very homogeneous size distribution of around 5−6 nm in diameter.

Similar results were obtained when nanodiscs were prepared from DPPC lipids (Figure 5B and Table 4). Although within this series, there was slightly more variation in size, again no obvious dependence on the fragment length was observed. We noted, however, that there can be some variation in particle sizes between independently prepared sample batches. As illustrated in Figure 5C,D, DLS experiments on a separate series of DMPC- and DPPC-derived samples showed a similar result for DMPC, but a somewhat larger nanodisc size for DPPC (Table 4), which was confirmed by EM characterization (Figure 6). We do not know the origin of this variation, but it likely arises from small differences in experimental procedures. The sizes are well within the range reported for these systems under similar conditions.[5,13,44,45] Importantly, within each of these series, there is no size difference based on the copolymer length. Moreover, in all series of experiments, the copolymers in this study give similar outcomes as Xiran 30010, both in

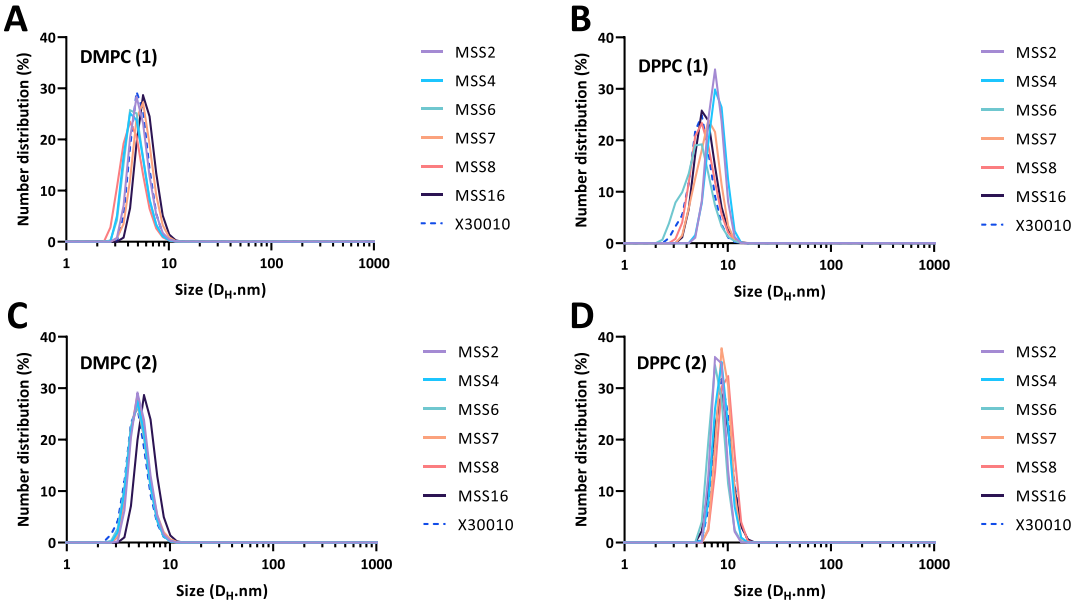

Figure 5. Number size distributions of nanoparticles as determined by DLS. SMA-bounded nanodiscs were obtained at a polymer-to-lipid mass ratio of 3, using either (A,C) DMPC or (B,D) DPPC lipids, prepared in two independent batches.

https://dx.doi.org/10.1021/acs.biomac.0c00736
Biomacromolecules 2020, 21, 3287−3300

Table 4. Size Distribution of Nanodiscs Prepared Using DMPC or DPPC Lipids, from Two Independent Batches and Analyzed Using DLS or TEM

	MSS2	MSS4	MSS6	MSS7	MSS8	MSS16	Xiran 30010
DMPC (1) DLS Size (D_H nm)	5.2 ± 1.2	4.8 ± 1.2	4.8 ± 1.2	5.7 ± 1.3	4.5 ± 1.2	6.1 ± 1.3	5.3 ± 1.1
DMPC (2) DLS Size (D_H nm)	5.3 ± 1.1	5.1 ± 1.1	5.0 ± 1.1	5.2 ± 1.3	5.1 ± 1.1	6.0 ± 1.3	4.9 ± 1.2
DPPC (1) DLS Size (D_H nm)	8.3 ± 1.2	8.8 ± 1.4	8.0 ± 1.3	9.2 ± 1.3	9.7 ± 1.6	9.0 ± 1.8	9.2 ± 1.7
DPPC (2) DLS Size (D_H nm)	7.6 ± 1.3	7.9 ± 1.5	5.2 ± 1.6	6.6 ± 1.5	5.9 ± 1.6	6.3 ± 1.5	5.6 ± 1.5
DPPC (1) EM Size (d nm)	8.7 ± 2.0	9.5 ± 1.8	9.5 ± 2.1	9.4 ± 2.5	9.9 ± 1.8	10.1 ± 2.2	8.7 ± 2.4

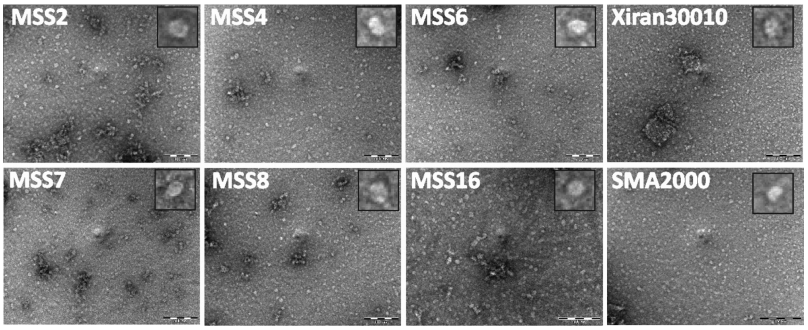

Figure 6. Negative-staining TEM images of DPPC (1) nanodiscs bounded by synthesized SMA copolymers. Nanoparticles were obtained at a SMA-to-lipid mass ratio of ∼3. The nanodiscs are discoidal in shape and have a diameter of ∼9 nm. Scale bars represent 100 nm. Insets are enlarged views of individual particles.

terms of the average size and heterogeneity (Table 4). Together, these results thus show that SMA copolymer length dispersity does not translate into size dispersity of the nanodiscs.

Previously, it was shown that the size distribution of nanodiscs can be affected by the concentration of SMA copolymers relative to lipid. This was also observed for the RAFT SMA copolymers studied here (Figure S10) with lower SMA concentrations giving rise to larger particle sizes.

Particles Stabilized by Larger Copolymers Have Better Stability in Terms of Lipid Exchange. The stability of the nanodiscs was investigated based on their lipid exchange rates. This was done at two different ionic strengths. Figure 7 shows that in both cases the longest fragments show the slowest exchange, suggesting that nanodiscs wrapped by larger copolymers have a higher stability. Indeed, when the time required to achieve 50% of total lipid exchange is plotted against polymer size, a linear relationship is observed (Figure S11). After 15 min, all copolymers reach the same extent of lipid exchange, corresponding to complete mixing. At a low salt concentration (Figure 7A), the rate of lipid exchange is slower as compared to higher salt concentrations (Figure 7B). This phenomenon has been observed before[15] and is attributed to fewer particle collisions at low salt concentrations because of the reduced charge screening. Furthermore, faster exchange kinetics were observed when using a larger excess of unlabeled nanodiscs (Figure S12), as also shown previously,[13,46] indicating that the exchange involves particle collisions. Remarkably, for all RAFT-synthesized copolymers, faster fluorescence dequenching times were observed than for Xiran 30010. The likely reasons for this will be further discussed below.

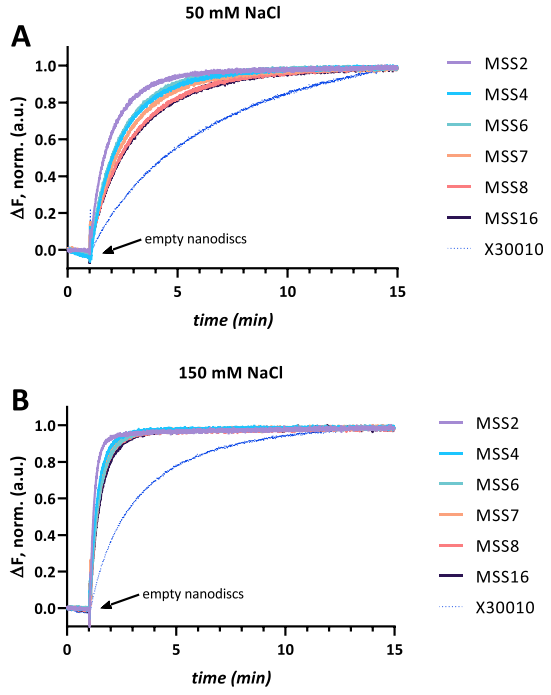

Figure 7. Fluorescence dequenching of rhodamine-PE (20 mol %) incorporated in DMPC nanodiscs with time upon the addition of unlabeled ("empty") nanodiscs. Experiments were recorded for 15 min with λ_{ex} = 560 nm and λ_{em} = 592 nm at 30 °C. Nanodiscs were mixed in a ratio of 5:1 (mol/mol) empty nanodiscs/fluorophore-loaded nanodiscs in a buffer system containing salt at a concentration of either (A) 50 mM NaCl or (B) 150 mM NaCl.

DISCUSSION AND CONCLUSIONS

SMAnh (2:1) Periodic Copolymer Synthesis and Characterization. Through the use of RAFT-mediated polymerization, it is possible to create polymers with a very narrow chain length distribution ($Đ$). In the case of SMA, this works well for the synthesis of alternating 1:1 copolymers (altSMA) or otherwise (2:1, 3:1) block copolymers of altSMA followed by polystyrene tails. In a CSTR, using conventional radical polymerization, one can make statistical 2:1 SMA (coSMA) with a narrow CCD but with a relatively high chain

https://dx.doi.org/10.1021/acs.biomac.0c00736
Biomacromolecules 2020, 21, 3287−3300

length dispersity ($Đ$). In this work, through the use of RAFT-mediated polymerization and an iterative addition process, it was possible to create coSMA polymers that have well-defined sizes of relatively low dispersity ($Đ$) and a fairly narrow CCD with an average STY/MAnh ratio of 2:1. There are two complications that limit the degree of control over this polymerization process. The first one is the necessity to use a relatively large amount of initiators, which is required to reach high STY conversion after each iterative chain extension step. This leads to an inevitable broadening of the MMD with increasing number of iterative steps. The second one is the statistical nature of the copolymerization, which limits the degree of control over the monomer sequence distribution. In depth kinetic analyses beyond the scope of this contribution are needed to get detailed insights into the chain growth process. Overall, the newly synthesized copolymers to our knowledge are still the best-defined 2:1 coSMA polymers made to date, in terms of chain-length dispersity and CCD. Notably, the only possibility so far to study copolymers with a precisely defined length and sequence has been through the use of molecular dynamics simulations.[47−49]

Spectroscopic analyses confirmed the SMA character of the newly synthesized copolymers when compared to the commercially available variant. Interestingly, when comparing the UV spectra, specifically in the relative intensities at 239 to 259 nm (valley-to-peak ratios), there is a difference between Xiran 30010 and the newly synthesized copolymers. For the RAFT copolymers, a lower ratio is found, which suggests that less contaminants may be present. How this may be of importance to the membrane active properties is discussed in the following sections.

Extent of Lipid Membrane Insertion Is Not the Rate-Limiting Step in Solubilization by (RAFT-Synthesized Nonalternating) SMA Copolymers. The monolayer experiments showed that there is no effect of the polymer length on monolayer insertion. This contrasts with the results of previous experiments, in which SMA length fractions were obtained by differential solubilizations of Xiran 30010 in organic solvents and where insertion of smaller fractions led to a higher final surface pressure.[13] The cause of this discrepancy is not clear at this point, but there may be several possible reasons. These include the presence of the end-groups in the RAFT-synthesized copolymers, the presence of contaminants in commercial mixtures that are absent or less abundant in the RAFT-synthesized copolymers, and subtle differences of the comonomer composition, such as the presence and length of styrene sequences. Further investigation would be required to find out the exact cause of the discrepancy with SMA fractions derived from Xiran 30010.

Our experiments furthermore showed that all RAFT-synthesized SMA copolymers are capable of solubilizing lipid membranes. Smaller polymers were found to have faster solubilization kinetics, consistent with results from the literature.[13] However, this cannot be ascribed to differences in the extent of insertion because no clear length-dependent differences were observed in the monolayer experiments, as discussed above. How then could we rationalize this? At first sight, a higher efficiency of membrane solubilization for shorter polymers even seems counterintuitive. This is because nanodisc formation will require a concerted effort of monomeric units of SMA polymers to disrupt the bilayer and to form nanodiscs, implying that longer polymers should be more efficient. Furthermore, in all cases, the length of the polymers is still smaller than the circumference of the nanodiscs. Therefore, multiple polymers are required to stabilize a single disc, and hence, larger polymers may be expected to be more effective. In spite of this, a higher efficiency of nanodisc formation by shorter polymers was observed. We speculate that the following two factors may explain this finding. First, an increase in the length of the copolymers also increases the risk of polymer entanglement on the surface of the membrane. This may hamper the required concerted action for nanodisc formation, without necessarily affecting monolayer insertion of the styrene units. Second, the longer the polymers are, the easier they could become involved in more than one event of nanodisc formation at the same time, thereby decreasing the efficiency of the process. Thus, the rate-limiting factor of membrane solubilization is not simply determined by the extent of insertion of SMA styrene units in the bilayer.

Polymer Size Does Not Translate into the Nanodisc Size. In all measurements, particle sizes were found to range between 5 and 10 nm in diameter. Although there was a small variation between different batches, the magnitude is well in agreement with nanodiscs from previous studies using a wide variety of lipids with different acyl chain lengths, head groups, and degree of unsaturation.[5,13,17,44] The results of DLS and TEM were found to be in good agreement with one another, which is encouraging, considering that negative stain TEM is performed on dehydrated samples and that in DLS the hydrodynamic size is calculated based on diffusion coefficients with the assumption of spherical particles.

No correlation was found between the size of the copolymer molecules and the size of the resulting nanodiscs, in agreement with previous results on SMA copolymers of different lengths.[13,50] Thus, the use of smaller copolymers presumably just requires a higher number of these polymers to shield the lipid acyl chains and form disc-like nanoparticles as compared to when using longer copolymers.

Thus far, only two factors have been reported to influence the nanodisc size. These are the compositions of the copolymer[15,50−53] and, as also shown in the present study, the ratio of polymer to lipid.[46,54,55] Intriguingly, previous studies even have found no relation between the size of encapsulated MPs and their respective nanodisc sizes.[56] The size of protein-encapsulated native nanodiscs was found to be around 13 nm in diameter for a relatively small protein with 7 transmembrane helices[4,57] and for a large supercomplex containing 48 transmembrane helices.[11] Together with our findings on the newly synthesized polymers as studied here, it thus seems unlikely that the polymer length will affect the size of protein encapsulated nanodiscs when applied to biological membranes. Whether and how the length of the polymers affects the extraction efficiency in native membranes or the stability of the encapsulated MPs remains to be investigated.

Copolymer Properties Shape Nanodisc Stability. The exchange rate of lipids was found to be influenced by the copolymer length, with larger copolymers resulting in nanodiscs that displayed slower lipid exchange. Because the size of the nanodiscs was found to be independent of the length of the copolymers, differences in the exchange rate cannot simply be attributed to differences in the number of particles and hence the number of collisions, but rather they should be ascribed to the number of successful collisions in terms of lipid exchange. We propose that collisions of nanodiscs with shorter polymers are more successful because of a lower stability of the

https://dx.doi.org/10.1021/acs.biomac.0c00736
Biomacromolecules 2020, 21, 3287−3300

nanoparticles. It should be noted here that nanodiscs are very dynamic structures, as in addition to transfer of lipids, exchange of copolymer molecules themselves has also been observed.[41] It could therefore be interesting to study if copolymer exchange is dependent on the copolymer length and whether longer copolymers perhaps might be more tightly bound, thereby better stabilizing the nanodiscs.

In addition to the copolymer size, it has also been found that average composition, that is, 2:1 versus 3:1 STY/MA plays an important role.[13] The faster exchange rates that we observed for RAFT-synthesized SMA copolymers as compared to Xiran 30010 suggests that stability may be further affected by the exact sequence distribution of the comonomers along the copolymer and in particular the content of SSS triads, which is higher in the RAFT-synthesized SMA (see Table 3) and which could potentially act as a hydrophobic carrier for the transfer of lipids. However, also factors such as the RAFT end-groups present on the copolymers, length dispersity, and contaminant molecules may play a role.

Finally, we would like to note that although lipid nanodiscs as studied here exhibit (rapid) lipid exchange,[46,58] for protein-containing native nanodiscs it was shown that they are able to retain an enrichment in certain lipid species for particular MPs.[7,59,60] This suggests that such lipids are more tightly bound as a result of specific protein−lipid interactions, and hence, that native nanodiscs formed by SMA copolymers can be a convenient tool to study such relationships.[9,11,61]

Comparison to Previously Synthesized RAFT SMA (Alternating Block Copolymers). Previous studies on SMA synthesized via RAFT polymerization have focused on so-called block copolymers, consisting of a block of alternating styrene−maleic acid (SMA) with the styrene excess forming a polystyrene tail. Because of this large difference in chain topology with the current nonalternating 2:1 SMA, a direct comparison is difficult. However, all of the various subtypes of RAFT SMA copolymers synthesized so far were found to be capable of lipid membrane solubilization into nanodiscs and to exhibit other characteristic properties of alternating SMA polymers. For example, it was shown for these block copolymers that the size of the nanoparticles can be modified by titrating the ratio of copolymer to lipid,[23] that smaller copolymers are better membrane solubilizers,[22] and that MPs can be incorporated and studied.[23] Furthermore, it was found that the size of the nanodiscs varies depending on the CCD of the polymers.[24] Importantly, Smith et al. probed the role of compositional gradient, and they found that styrene homoblocks are mostly detrimental to protein solubilization.[22]

Besides a better defined MMD, another advantage of RAFT-synthesized copolymers is their potential for conjugation chemistry. By hydrolyzing the terminal RAFT moiety to its free thiol, it is possible to selectively functionalize the copolymer end, that is, attach a single fluorophore or an affinity tag to every polymer chain. An example of this coupling is through facile thiol-maleimide conjugation, as performed by Smith et al.[22] If the RAFT end-group is not cleaved, then it may be important to consider which RAFT agent is employed. For example, especially when the copolymer is relatively short, the total mass and the physico-chemical properties of the copolymers can be strongly affected by whether the RAFT copolymer end is a phenyl, dodecyl, or butyl group.

In addition to the modification of the copolymer end-groups in RAFT copolymers, all styrene−maleic anhydride copolymers can be modified on the maleic anhydride monomeric units. Recently, Burridge et al. derivatized RAFT SMA groups in such a fashion in order to produce nanodiscs that were stable against a wide range of pH and high divalent cation concentrations, and they showed that these modified RAFT SMA were capable of solubilizing the MP KCNE1.[25]

Prospects. Through the use of RAFT-mediated synthesis, researchers will be able to obtain better defined SMA copolymers. This is certainly true in terms of the copolymer size distribution, although the RAFT-mediated synthesis of well-defined sequence-controlled nonalternating SMA is still a challenge, as shown in the present study. RAFT-synthesized copolymers furthermore have the advantage that they lend well to chemical modification in a more controlled manner and the use of RAFT SMA is clearly showing promise for the solubilization of membranes as well as MPs. Therefore, RAFT SMA potentially offers an economical alternative to some commercial products. Well-defined SMA copolymers of different lengths, such as those used in the present study, will thus offer many intriguing possibilities to gain further insights into how SMA copolymers solubilize different types of membranes and how they affect the properties of nanodiscs.

■ ASSOCIATED CONTENT

Supporting Information

The Supporting Information is available free of charge at https://pubs.acs.org/doi/10.1021/acs.biomac.0c00736.

Calculation of dead chain fraction; ^{1}H NMR spectrum of the RAFT agent; UV−vis spectra of SMAnh copolymers; SEC traces of SMAnh copolymers; ^{1}H and ^{13}C DEPT NMR spectra of SMAnh copolymers; ATR−FTIR spectra of SMA copolymers; digital picture of SMA copolymer solutions; surface pressure of aqueous SMA copolymer solution; correlation between bilayer insertion and the SMA chain length; optical density after 340 s of exposing a lipid dispersion as a function of the SMA chain length; number size distribution of nanodiscs as measured by DLS for MSS2 at different polymer to lipid ratios; time to reach 50% lipid exchange as a function of the SMA chain length; and lipid exchange experiment as measured by fluorescence spectroscopy for different SMA chain lengths (PDF)

■ AUTHOR INFORMATION

Corresponding Authors

J. Antoinette Killian − *Membrane Biochemistry & Biophysics, Bijvoet Center for Biomolecular Research and Institute of Biomembranes, Utrecht University, Utrecht 3584 CH, the Netherlands*; Email: j.a.killian@uu.nl

Bert Klumperman − *Department of Chemistry and Polymer Science, Stellenbosch University, Matieland 7602, South Africa*; orcid.org/0000-0003-1561-274X; Email: bklump@sun.ac.za

Authors

Randy D. Cunningham − *Department of Chemistry and Polymer Science, Stellenbosch University, Matieland 7602, South Africa*

Adrian H. Kopf − *Membrane Biochemistry & Biophysics, Bijvoet Center for Biomolecular Research and Institute of Biomembranes, Utrecht University, Utrecht 3584 CH, the Netherlands*

Barend O. W. Elenbaas − *Membrane Biochemistry & Biophysics, Bijvoet Center for Biomolecular Research and Institute of Biomembranes, Utrecht University, Utrecht 3584 CH, the Netherlands*

Bastiaan B.P. Staal − *BASF SE, RAA/AC, E210, Ludwigshafen am Rhein 67056, Germany*

Rueben Pfukwa − *Department of Chemistry and Polymer Science, Stellenbosch University, Matieland 7602, South Africa*

Complete contact information is available at: https://pubs.acs.org/10.1021/acs.biomac.0c00736

Author Contributions

[‖]R.D.C. and A.H.K. are equal contributions.

Notes

The authors declare no competing financial interest.

■ ACKNOWLEDGMENTS

We thank Martijn C. Koorengevel and Cornelis van Walree for helpful discussions, Bonny W. M. Kuipers for the support in DLS analysis, and Polyscope Polymers for providing the commercially available SMAnh (Xiran SZ 30010) copolymer as a kind gift. This work was supported financially by the Division of Chemical Sciences (CW) of the Netherlands Organisation for Scientific Research (NWO), via ECHO grants no. 711-017-006 (A.H.K). This work further based on research supported by the South African Research Chairs Initiative of the Department of Science and Technology (DST) and National Research Foundation (NRF) of South Africa (grant no. 46855).

■ ABBREVIATIONS

SMA	styrene−maleic acid
SMALP	SMA lipid particle
SMAnh	styrene−maleic anhydride
MP	membrane protein
CCD	chemical composition distribution
MMD	molecular mass distribution
Đ	dispersity
CSTR	continuous stirred tank reactor
DEPT	distortionless enhancement by polarization transfer
S	styrene
M	maleic acid
RAFT	reversible addition−fragmentation chain-transfer
RDRP	reversible-deactivation radical polymerization
M_n	number-average molecular weight
DP	degree of polymerization
T_m	(gel-to-fluid crystalline) phase transition temperature
MLV	multilamellar vesicle
AIBN	2,2′-azobis(2-methylpropionitrile)
BPT	butyl-(1-phenyl ethyl) trithiocarbonate
X30010	Xiran 30010
DMPC	1,2-dimyristoyl-*sn*-glycero-3-phosphocholine
DPPC	1,2-dipalmitoyl-*sn*-glycero-3-phosphocholine
DSPC	1,2-distearoyl-*sn*-glycero-3-phosphocholine
DLS	dynamic light scattering
TEM	transmission electron microscopy
NMR	nuclear magnetic resonance
NOE	nuclear Overhauser enhancement
ATR−FTIR	attenuated total reflectance Fourier-transform IR spectroscopy
UV−vis	ultraviolet−visible
SEC	size exclusion chromatography

■ REFERENCES

(1) Stetsenko, A.; Guskov, A. An Overview of the Top Ten Detergents Used for Membrane Protein Crystallization. *Crystals* **2017**, *7*, 197.

(2) Stroud, Z.; Hall, S. C. L.; Dafforn, T. R. Purification of Membrane Proteins Free from Conventional Detergents: SMA, New Polymers, New Opportunities and New Insights. *Methods* **2018**, *147*, 106−117.

(3) Overduin, M.; Klumperman, B. Advancing Membrane Biology with Poly(Styrene-Co-Maleic Acid)-Based Native Nanodiscs. *Eur. Polym. J.* **2019**, *110*, 63−68.

(4) Knowles, T. J.; Finka, R.; Smith, C.; Lin, Y.-P.; Dafforn, T.; Overduin, M. Membrane Proteins Solubilized Intact in Lipid Containing Nanoparticles Bounded by Styrene Maleic Acid Copolymer. *J. Am. Chem. Soc.* **2009**, *131*, 7484−7485.

(5) Scheidelaar, S.; Koorengevel, M. C.; Pardo, J. D.; Meeldijk, J. D.; Breukink, E.; Killian, J. A. Molecular Model for the Solubilization of Membranes into Nanodisks by Styrene Maleic Acid Copolymers. *Biophys. J.* **2015**, *108*, 279−290.

(6) Jamshad, M.; Grimard, V.; Idini, I.; Knowles, T. J.; Dowle, M. R.; Schofield, N.; Sridhar, P.; Lin, Y.; Finka, R.; Wheatley, M.; Thomas, O. R. T.; Palmer, R. E.; Overduin, M.; Govaerts, C.; Ruysschaert, J.-M.; Edler, K. J.; Dafforn, T. R. Structural Analysis of a Nanoparticle Containing a Lipid Bilayer Used for Detergent-Free Extraction of Membrane Proteins. *Nano Res.* **2015**, *8*, 774−789.

(7) Dörr, J. M.; Koorengevel, M. C.; Schäfer, M.; Prokofyev, A. V.; Scheidelaar, S.; Van Der Cruijsen, E. A. W.; Dafforn, T. R.; Baldus, M.; Killian, J. A. Detergent-Free Isolation, Characterization, and Functional Reconstitution of a Tetrameric K+ Channel: The Power of Native Nanodiscs. *Proc. Natl. Acad. Sci. U.S.A.* **2014**, *111*, 18607−18612.

(8) Qiu, W.; Fu, Z.; Xu, G. G.; Grassucci, R. A.; Zhang, Y.; Frank, J.; Hendrickson, W. A.; Guo, Y. Structure and Activity of Lipid Bilayer within a Membrane-Protein Transporter. *Proc. Natl. Acad. Sci. U.S.A.* **2018**, *115*, 12985−12990.

(9) Calzada, E.; Avery, E.; Sam, P. N.; Modak, A.; Wang, C.; McCaffery, J. M.; Han, X.; Alder, N. N.; Claypool, S. M. Phosphatidylethanolamine Made in the Inner Mitochondrial Membrane Is Essential for Yeast Cytochrome Bc 1 Complex Function. *Nat. Commun.* **2019**, *10*, 1−17.

(10) Parmar, M.; Rawson, S.; Scarff, C. A.; Goldman, A.; Dafforn, T. R.; Muench, S. P.; Postis, V. L. G. Using a SMALP Platform to Determine a Sub-Nm Single Particle Cryo-EM Membrane Protein Structure. *Biochim. Biophys. Acta Biomembr.* **2018**, *1860*, 378−383.

(11) Sun, C.; Benlekbir, S.; Venkatakrishnan, P.; Wang, Y.; Hong, S.; Hosler, J.; Tajkhorshid, E.; Rubinstein, J. L.; Gennis, R. B. Structure of the Alternative Complex Lll in a Supercomplex with Cytochrome Oxidase. *Nature* **2018**, *557*, 123−126.

(12) Morrison, K. A.; Akram, A.; Mathews, A.; Khan, Z. A.; Patel, J. H.; Zhou, C.; Hardy, D. J.; Moore-Kelly, C.; Patel, R.; Odiba, V.; Knowles, T. J.; Javed, M.-u. -H.; Chmel, N. P.; Dafforn, T. R.; Rothnie, A. J. Membrane Protein Extraction and Purification Using Styrene-Maleic Acid (SMA) Copolymer: Effect of Variations in Polymer Structure. *Biochem. J.* **2016**, *473*, 4349−4360.

(13) Pardo, J. J. D.; Koorengevel, M. C.; Uwugiaren, N.; Weijers, J.; Kopf, A. H.; Jahn, H.; van Walree, C. A.; van Steenbergen, M. J.; Killian, J. A. Membrane Solubilization by Styrene-Maleic Acid Copolymers: Delineating the Role of Polymer Length. *Biophys. J.* **2018**, *115*, 129−138.

(14) Swainsbury, D. J. K.; Scheidelaar, S.; Foster, N.; van Grondelle, R.; Killian, J. A.; Jones, M. R. The Effectiveness of Styrene-Maleic Acid (SMA) Copolymers for Solubilisation of Integral Membrane Proteins from SMA-Accessible and SMA-Resistant Membranes. *Biochim. Biophys. Acta Biomembr.* **2017**, *1859*, 2133−2143.

(15) Grethen, A.; Oluwole, A. O.; Danielczak, B.; Vargas, C.; Keller, S. Thermodynamics of Nanodisc Formation Mediated by Styrene/Maleic Acid (2:1) Copolymer. *Sci. Rep.* **2017**, *7*, 1−14.
(16) Scheidelaar, S.; Koorengevel, M. C.; van Walree, C. A.; Dominguez, J. J.; Dörr, J. M.; Killian, J. A. Effect of Polymer Composition and PH on Membrane Solubilization by Styrene-Maleic Acid Copolymers. *Biophys. J.* **2016**, *111*, 1974−1986.
(17) Dominguez Pardo, J. J.; Dörr, J. M.; Renne, M. F.; Ould-Braham, T.; Koorengevel, M. C.; van Steenbergen, M. J.; Killian, J. A. Thermotropic Properties of Phosphatidylcholine Nanodiscs Bounded by Styrene-Maleic Acid Copolymers. *Chem. Phys. Lipids* **2017**, *208*, 58−64.
(18) Gulamhussein, A. A.; Meah, D.; Soja, D. D.; Fenner, S.; Saidani, Z.; Akram, A.; Lallie, S.; Mathews, A.; Painter, C.; Liddar, M. K.; Mohammed, Z.; Chiu, L. K.; Sumar, S. S.; Healy, H.; Hussain, N.; Patel, J. H.; Hall, S. C. L.; Dafforn, T. R.; Rothnie, A. J. Examining the Stability of Membrane Proteins within SMALPs. *Eur. Polym. J.* **2019**, *112*, 120−125.
(19) Benoit, D.; Hawker, C. J.; Huang, E. E.; Lin, Z.; Russell, T. P. One-Step Formation of Functionalized Block Copolymers. *Macromolecules* **2000**, *33*, 1505−1507.
(20) Lessard, B.; Marić, M. One-Step Poly(Styrene-Alt-Maleic Anhydride)-Block-Poly(Styrene) Copolymers with Highly Alternating Styrene/Maleic Anhydride Sequences Are Possible by Nitroxide-Mediated Polymerization. *Macromolecules* **2010**, *43*, 879−885.
(21) De Brouwer, H.; Schellekens, M. A. J.; Klumperman, B.; Monteiro, M. J.; German, A. L. Controlled Radical Copolymerization of Styrene and Maleic Anhydride and the Synthesis of Novel Polyolefin-Based Block Copolymers by Reversible Addition-Fragmentation Chain-Transfer (RAFT) Polymerization. *J. Polym. Sci., Part A: Polym. Chem.* **2000**, *38*, 3596−3603.
(22) Smith, A. A. A.; Autzen, H. E.; Laursen, T.; Wu, V.; Yen, M.; Hall, A.; Hansen, S. D.; Cheng, Y.; Xu, T. Controlling Styrene Maleic Acid Lipid Particles through RAFT. *Biomacromolecules* **2017**, *18*, 3706−3713.
(23) Harding, B. D.; Dixit, G.; Burridge, K. M.; Sahu, I. D.; Dabney-Smith, C.; Edelmann, R. E.; Konkolewicz, D.; Lorigan, G. A. Characterizing the Structure of Styrene-Maleic Acid Copolymer-Lipid Nanoparticles (SMALPs) Using RAFT Polymerization for Membrane Protein Spectroscopic Studies. *Chem. Phys. Lipids* **2019**, *218*, 65−72.
(24) Hall, S. C. L.; Tognoloni, C.; Price, G. J.; Klumperman, B.; Edler, K. J.; Dafforn, T. R.; Arnold, T. Influence of Poly(Styrene- Co -Maleic Acid) Copolymer Structure on the Properties and Self-Assembly of SMALP Nanodiscs. *Biomacromolecules* **2018**, *19*, 761−772.
(25) Burridge, K. M.; Harding, B. D.; Sahu, I. D.; Kearns, M. M.; Stowe, R. B.; Dolan, M. T.; Edelmann, R. E.; Dabney-Smith, C.; Page, R. C.; Konkolewicz, D.; Lorigan, G. A. Simple Derivatization of RAFT-Synthesized Styrene-Maleic Anhydride Copolymers for Lipid Disk Formulations. *Biomacromolecules* **2020**, *21*, 1274−1284.
(26) Knowles, T. J.; Finka, R.; Smith, C.; Lin, Y.-P.; Dafforn, T.; Overduin, M. Membrane Proteins Solubilized Intact in Lipid Containing Nanoparticles Bounded by Styrene Maleic Acid Copolymer. *J. Am. Chem. Soc.* **2009**, *131*, 7484−7485.
(27) Jamshad, M.; Lin, Y.-P.; Knowles, T. J.; Parslow, R. A.; Harris, C.; Wheatley, M.; Poyner, D. R.; Bill, R. M.; Thomas, O. R. T.; Overduin, M.; Dafforn, T. R. Surfactant-Free Purification of Membrane Proteins with Intact Native Membrane Environment. *Biochem. Soc. Trans.* **2011**, *39*, 813−818.
(28) Postma, A.; Davis, T. P.; Evans, R. A.; Li, G.; Moad, G.; O'Shea, M. S. Synthesis of Well-Defined Polystyrene with Primary Amine End Groups through the Use of Phthalimido-Functional RAFT Agents. *Macromolecules* **2006**, *39*, 5293−5306.
(29) Barron, P. F.; Poly, C.; Hil, D. J. T.; Donnell, J. H. O.; Sullivan, P. W. O. Applications of DEPT Experiments to the 13C. *Macromolecules* **1984**, *17*, 1967−1972.
(30) Kopf, A. H.; Koorengevel, M. C.; van Walree, C. A.; Dafforn, T. R.; Killian, J. A. A Simple and Convenient Method for the Hydrolysis of Styrene-Maleic Anhydride Copolymers to Styrene-Maleic Acid Copolymers. *Chem. Phys. Lipids* **2019**, *218*, 85−90.
(31) Lewis, R. N. A. H.; Mak, N.; McElhaney, R. N. A Differential Scanning Calorimetric Study of the Thermotropic Phase Behavior of Model Membranes Composed of Phosphatidylcholines Containing Linear Saturated Fatty Acyl Chains. *Biochemistry* **1987**, *26*, 6118−6126.
(32) Huang, J.; Turner, S. R. Recent Advances in Alternating Copolymers: The Synthesis, Modification, and Applications of Precision Polymers. *Polym* **2017**, *116*, 572−586.
(33) Klumperman, B. Mechanistic Considerations on Styrene−Maleic Anhydride Copolymerization Reactions. *Polym. Chem.* **2010**, *1*, 558−562.
(34) Charpentier, P. A.; DeSimone, J. M.; Roberts, G. W. Decomposition of Polymerization Initiators in Supercritical CO2: A Novel Approach to Reaction Kinetics Using a CSTR. *Chem. Eng. Sci.* **2000**, *55*, 5341−5349.
(35) Gody, G.; Maschmeyer, T.; Zetterlund, P. B.; Perrier, S. Rapid and Quantitative One-Pot Synthesis of Sequence-Controlled Polymers by Radical Polymerization. *Nat. Commun.* **2013**, *4*, 1−9.
(36) Gody, G.; Zetterlund, P. B.; Perrier, S.; Harrisson, S. The Limits of Precision Monomer Placement in Chain Growth Polymerization. *Nat. Commun.* **2016**, *7*, 1−8.
(37) Klumperman, L. Free Radical Copolymerization of Styrene and Maleic Anhydride: Kinetic Studies at Low and Intermediate Conversion. Ph.D. Thesis, Eindhoven University of Technology, 1994.
(38) van den Dungen, E. T. A.; Rinquest, J.; Pretorius, N. O.; McKenzie, J. M.; McLeary, J. B.; Sanderson, R. D.; Klumperman, B. Investigation into the Initialization Behaviour of RAFT-Mediated Styrene-Maleic Anhydride Copolymerizations. *Aust. J. Chem.* **2006**, *59*, 742−748.
(39) Banerjee, S.; Pal, T. K.; Guha, S. K. Probing Molecular Interactions of Poly(Styrene-Co-Maleic Acid) with Lipid Matrix Models to Interpret the Therapeutic Potential of the Co-Polymer. *Biochim. Biophys. Acta Biomembr.* **2012**, *1818*, 537−550.
(40) Jamshad, M.; Charlton, J.; Lin, Y.; Routledge, S. J.; Bawa, Z.; Knowles, T. J.; Overduin, M.; Dekker, N.; Dafforn, T. R.; Bill, R. M.; Poyner, D. R.; Wheatley, M. G-Protein Coupled Receptor Solubilization and Purification for Biophysical Analysis and Functional Studies, in the Total Absence of Detergent. *Biosci. Rep.* **2015**, *35*, 1−10.
(41) Schmidt, V.; Sturgis, J. N. Modifying Styrene-Maleic Acid Co-Polymer for Studying Lipid Nanodiscs. *Biochim. Biophys. Acta Biomembr.* **2018**, *1860*, 777−783.
(42) Boisselier, É.; Calvez, P.; Demers, É.; Cantin, L.; Salesse, C. Influence of the Physical State of Phospholipid Monolayers on Protein Binding. *Langmuir* **2012**, *28*, 9680−9688.
(43) Calvez, P.; Bussières, S.; Demers, É.; Salesse, C. Parameters Modulating the Maximum Insertion Pressure of Proteins and Peptides in Lipid Monolayers. *Biochimie* **2009**, *91*, 718−733.
(44) Pardo, J. J. D.; Dörr, J. M.; Iyer, A.; Cox, R. C.; Scheidelaar, S.; Koorengevel, M. C.; Subramaniam, V.; Killian, J. A. Solubilization of Lipids and Lipid Phases by the Styrene−Maleic Acid Copolymer. *Eur. Biophys. J.* **2017**, *46*, 91−101.
(45) Dominguez Pardo, J. J.; Dörr, J. M.; Renne, M. F.; Ould-Braham, T.; Koorengevel, M. C.; van Steenbergen, M. J.; Killian, J. A. Thermotropic Properties of Phosphatidylcholine Nanodiscs Bounded by Styrene-Maleic Acid Copolymers. *Chem. Phys. Lipids* **2017**, *208*, 58−64.
(46) Arenas, R. C.; Danielczak, B.; Martel, A.; Porcar, L.; Breyton, C.; Ebel, C.; Keller, S. Fast Collisional Lipid Transfer among Polymer-Bounded Nanodiscs. *Sci. Rep.* **2017**, *7*, 1−8.
(47) Xue, M.; Cheng, L.; Faustino, I.; Guo, W.; Marrink, S. J. Molecular Mechanism of Lipid Nanodisk Formation by Styrene-Maleic Acid Copolymers. *Biophys. J.* **2018**, *115*, 494−502.
(48) Orekhov, P. S.; Bozdaganyan, M. E.; Voskoboynikova, N.; Mulkidjanian, A. Y.; Steinhoff, H.-J.; Shaitan, K. V. Styrene/Maleic

Acid Copolymers Form SMALPs by Pulling Lipid Patches out of the Lipid Bilayer. *Langmuir* **2019**, *35*, 3748−3758.
(49) Colbasevici, A.; Voskoboynikova, N.; Orekhov, P. S.; Bozdaganyan, M. E.; Karlova, M. G.; Sokolova, O. S.; Klare, J. P.; Mulkidjanian, A. Y.; Shaitan, K. V.; Steinhoff, H.-J. Lipid Dynamics in Nanoparticles Formed by Maleic Acid-Containing Copolymers: EPR Spectroscopy and Molecular Dynamics Simulations. *Biochim. Biophys. Acta Biomembr.* **2020**, *1862*, 183207.
(50) Craig, A. F.; Clark, E. E.; Sahu, I. D.; Zhang, R.; Frantz, N. D.; Al-abdul-wahid, M. S.; Dabney-smith, C.; Konkolewicz, D.; Lorigan, G. A. Biochimica et Biophysica Acta Tuning the Size of Styrene-Maleic Acid Copolymer-Lipid Nanoparticles (SMALPs) Using RAFT Polymerization for Biophysical Studies. *Biochim. Biophys. Acta Biomembr.* **2016**, *1858*, 2931−2939.
(51) Ravula, T.; Hardin, N. Z.; Ramadugu, S. K.; Ramamoorthy, A. PH Tunable and Divalent Metal Ion Tolerant Polymer Lipid Nanodiscs. *Langmuir* **2017**, *33*, 10655−10662.
(52) Ravula, T.; Hardin, N. Z.; Bai, J.; Im, S.-C.; Waskell, L.; Ramamoorthy, A. Effect of Polymer Charge on Functional Reconstitution of Membrane Proteins in Polymer Nanodiscs. *Chem. Commun.* **2018**, *54*, 9615−9618.
(53) Hardin, N. Z.; Ravula, T.; Mauro, G. D.; Ramamoorthy, A. Hydrophobic Functionalization of Polyacrylic Acid as a Versatile Platform for the Development of Polymer Lipid Nanodisks. *Small* **2019**, *15*, 1804813.
(54) Zhang, R.; Sahu, I. D.; Liu, L.; Osatuke, A.; Comer, R. G.; Dabney-Smith, C.; Lorigan, G. A. Characterizing the Structure of Lipodisq Nanoparticles for Membrane Protein Spectroscopic Studies. *Biochim. Biophys. Acta Biomembr.* **2015**, *1848*, 329−333.
(55) Radoicic, J.; Park, S. H.; Opella, S. J. Macrodiscs Comprising SMALPs for Oriented Sample Solid-State NMR Spectroscopy of Membrane Proteins. *Biophys. J.* **2018**, *115*, 22−25.
(56) Dörr, J. M.; Scheidelaar, S.; Koorengevel, M. C.; Dominguez, J. J.; Schäfer, M.; van Walree, C. A.; Killian, J. A. The Styrene−Maleic Acid Copolymer: A Versatile Tool in Membrane Research. *Eur. Biophys. J.* **2016**, *45*, 3−21.
(57) Orwick-Rydmark, M.; Lovett, J. E.; Graziadei, A.; Lindholm, L.; Hicks, M. R.; Watts, A. Detergent-Free Incorporation of a Seven-Transmembrane Receptor Protein into Nanosized Bilayer Lipodisq Particles for Functional and Biophysical Studies. *Nano Lett.* **2012**, *12*, 4687−4692.
(58) Hazell, G.; Arnold, T.; Barker, R. D.; Clifton, L. A.; Steinke, N.-J.; Tognoloni, C.; Edler, K. J. Evidence of Lipid Exchange in Styrene Maleic Acid Lipid Particle (SMALP) Nanodisc Systems. *Langmuir* **2016**, *32*, 11845−11853.
(59) Schmidt, V.; Sidore, M.; Bechara, C.; Duneau, J.-P.; Sturgis, J. N. The Lipid Environment of Escherichia Coli Aquaporin Z. *Biochim. Biophys. Acta Biomembr.* **2019**, *1861*, 431−440.
(60) Prabudiansyah, I.; Kusters, I.; Caforio, A.; Driessen, A. J. M. Characterization of the Annular Lipid Shell of the Sec Translocon. *Biochim. Biophys. Acta Biomembr.* **2015**, *1848*, 2050−2056.
(61) Teo, A. C. K.; Lee, S. C.; Pollock, N. L.; Stroud, Z.; Hall, S.; Thakker, A.; Pitt, A. R.; Dafforn, T. R.; Spickett, C. M.; Roper, D. I. Analysis of SMALP Co-Extracted Phospholipids Shows Distinct Membrane Environments for Three Classes of Bacterial Membrane Protein. *Sci. Rep.* **2019**, *9*, 1−10.

https://dx.doi.org/10.1021/acs.biomac.0c00736
Biomacromolecules 2020, 21, 3287−3300